

# P-WILLMORE FLOW WITH QUASI-CONFORMAL MESH REGULARIZATION

ANTHONY GRUBER<sup>1</sup>, EUGENIO AULISA<sup>2</sup>,

**ABSTRACT.** The p-Willmore functional introduced in [1] unifies and extends important geometric functionals which measure the area, total mean curvature, and Willmore energy of immersed surfaces. Techniques from [2] are adapted to compute the first variation of the p-Willmore functional, which is then used to develop a finite-element model for the p-Willmore flow of closed surfaces in  $\mathbb{R}^3$  that is amenable to constraints on surface area and enclosed volume. Further, a minimization-based regularization procedure is formulated to prevent mesh degeneration along the flow. Inspired by a conformality condition derived in [3], this procedure is generally-applicable to all 2-D meshes and ensures that a given surface mesh remains nearly conformal as it evolves, at the expense of first-order accuracy in the flow. Finally, discretization of the p-Willmore flow is discussed, where some basic results on consistency and numerical stability are demonstrated and a fully-automated algorithm is presented for implementing the closed surface p-Willmore flow with mesh regularization.

## 1. INTRODUCTION

Geometric flows have proven themselves to be beautiful and powerful tools for solving important mathematical problems, including the famous Poincare conjecture [4]. Perhaps unsurprisingly, it turns out that many of these flows can be constructed from the  $L^2$ -gradient of a suitable energy functional, which often has physical as well as mathematical importance. For example, the mean curvature flow (MCF), defined in terms of the arithmetic mean of the principal curvatures, arises when considering deformations of a surface which decrease its overall area and has applications in capillary physics and fluid flow through porous media (see [5]). This is moreover quite natural on mathematical grounds, since the MCF can be easily expressed as surface evolution by (minus) the  $L^2$  gradient of the area functional.

As another example, the reliable Helfrich model for biomembranes (see [6]) is based on the well-studied Willmore energy (see [7, 8, 9, 10, 11, 12] and references therein)

$$(1) \quad \mathcal{W}^2(M) = \int_M H^2 dS,$$

whose  $L^2$ -gradient flow has been proven to converge to a global minimum when the surface genus and initial energy are sufficiently low [13, 14]. An example of this convergence is displayed in Figure 1. Due

---

Correspondence to: Anthony Gruber, Department of Mathematics and Statistics, Texas Tech University, Lubbock, TX 79409.  
E-mail address: anthony.gruber@ttu.edu.

to its pleasing aesthetic character, the Willmore flow has further attracted the interest of computational mathematicians and scientists, and has been studied numerically in a variety of contexts including conformal geometry, geometric PDE, and computer vision. See e.g. [15, 16, 17] and the references therein.



FIGURE 1. 2-Willmore evolution of a rough and asymmetric torus to a known global minimum. The minimizing surface is the stereographic projection of a Clifford torus in  $S^3$ .

**1.1. Related work.** Besides the inherent mathematical challenges present in geometric flows (involving e.g. convergence, changes in global topology, and singularity formation), these objects introduce a number of computational difficulties as well. In particular, computational surfaces are often stored as piecewise-linear data, such as meshes of simplices, and it is taxing to find a satisfactory method of expression for second-order geometric phenomena such as curvature. There have been two broad approaches to this problem in the current literature, which can be thought of colloquially as arising from *discrete* versus *discretized* perspectives on this issue.

In discrete geometry, the aim is to use global characterizations from geometry and topology to develop fully-discrete analogues of classical geometric quantities, which are in some sense independent from their original (continuous) definitions. Tools such as exterior calculus, the Gauss-Bonnet and Stokes' Theorems are employed to define length, area, curvature, etc. on a simplicial surface, which is accomplished through enforcing global geometric relationships rather than considering local values at specific places (nodes) on the mesh. The main advantages of this approach are relative independence from mesh quality, and sparse linear formulations which are fast to solve. Some notable disadvantages present here are the restriction of such methods (so far) to triangular meshes, and the fact that several equivalent definitions of geometric quantities in the smooth setting become inequivalent when treated in this way (see [18] for details). Further information on this area can be found in [19, 20, 21, 22, 23] and the references therein.

Conversely, discretized geometry involves approximating continuous geometric quantities as well as possible by using a good choice of nodal mesh points, so that the difference between the continuous and discrete objects vanishes in the limit of mesh refinement. Traditional finite element mathematics is based on this idea, whereby the necessary calculations are done locally and element-wise without any particular adherence to

global phenomena except in the limit. The primary advantage of this approach is its flexibility with respect to applications, problem formulations, and mesh data. Its main disadvantages are its inherent sensitivity to mesh quality, and its agnosticism with respect to the global aspects of surface geometry. See [16] for a compendium of knowledge and techniques in this area.

**Remark 1.1.** This failure of the finite element method to capture global relationships was in fact a primary motivation for the development of a discrete geometric theory, as mentioned in [22, 23].

The computational details of geometric flows have been examined previously from both of the above perspectives. In [2], the author studies parametric Willmore flow from a finite-element perspective. In particular, he develops and discretizes a model for the Willmore flow of surfaces, detailing some examples and proving consistency of the discretization. On the other hand, the authors in [18] use ideas from discrete conformal geometry to develop a fully-conformal model for the Willmore flow. More precisely, they develop results which enable the direct manipulation of surface curvature, allowing for angle-preserving mesh positions to be recovered using a natural integrability condition. Beyond the Willmore flow, many computational studies have also been done which focus on the mean and Gauss curvature flows, Ricci flow, and Yamabe flow of surfaces; see [24, 17] and their enclosed references for more details.

**1.2. Contributions.** This work adopts a discretized perspective similar to [16] and aims to extend the computational study of curvature flows. To that end, the main object of study is the  $L^2$ -gradient flow of the  $p$ -Willmore functional introduced in [1],

$$(2) \quad \mathcal{W}^p(M) = \frac{1}{2^p} \int_M H^p dS, \quad p \in \mathbb{Z}_{\geq 0}.$$

Note that the surface area, total mean curvature, and Willmore functionals are encompassed here as  $\mathcal{W}^0$ ,  $\mathcal{W}^1$ , and  $\mathcal{W}^2$ , respectively. It follows from this definition that the 0-Willmore flow is simply MCF, the 1-Willmore flow is the Gauss curvature flow (GCF), and the 2-Willmore flow is the usual Willmore flow. Since each of these flows has remarkably different geometric properties from the others, it is reasonable to desire a more general model. A notable advantage of the  $p$ -Willmore functional is that it can be used to examine the various similarities and differences present in flows that involve general powers  $p$  of the mean curvature. Examples of this are displayed in Figure 2 and Figure 10.

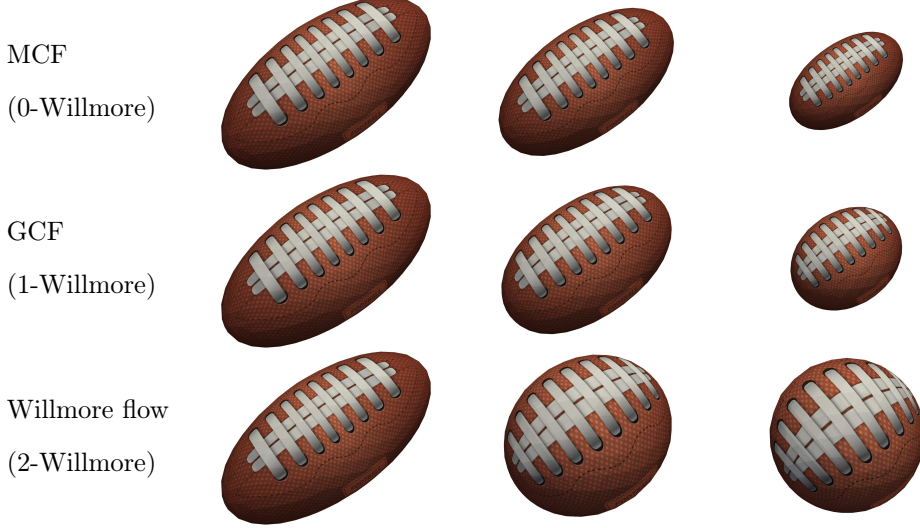


FIGURE 2. p-Willmore evolution of an ellipsoid when  $p = 0, 1, 2$  at comparable timescales.

In the following sections, techniques from [2] will be adapted to express the  $L^2$ -gradient of  $\mathcal{W}^p$  in a computationally-accessible way, resulting in an appropriate weak formulation of the p-Willmore flow problem. Once the relevant system of PDE has been established, geometric constraints on surface area and enclosed volume will be considered and introduced into the flow model as Lagrange multipliers, leading to new and different behavior. Moreover, the problem of mesh degradation along the flow will be discussed, and a minimization procedure will be given which dramatically improves mesh quality throughout the p-Willmore flow at the expense of first-order accuracy in the implementation. This procedure is inspired by a conformality criterion of Kamberov, Pedit, and Pinkall derived in [3] and is similar in spirit to the least squares conformal mapping (LSCM) technique introduced in [25]. Consequently, the p-Willmore flow and mesh regularization systems will be discretized and implemented on manifold meshes of triangles and quadrilaterals [26], where it will be shown that the discretized p-Willmore flow is energy-decreasing and stable in appropriate norms. Finally, a complete and fully-automated algorithm is presented for running the p-Willmore flow with mesh regularization.

The p-Willmore flow algorithm introduced here has the following benefits:

- It unifies and extends several known flows of interest: including MCF, GCF, and the Willmore flow.
- It is flexible with respect to geometric constraints on area and volume, as well as mesh geometry data (tri or quad) and surface genera.
- It affords the ability to quasi-conformally regularize the surface mesh along the flow, preventing mesh degeneration at the expense of first-order accuracy in the simulation.

- It is entirely minimization based and therefore amenable to a large library of developed theory and techniques.

**Remark 1.2.** Note that the term “quasi-conformal” is used here in a mathematically imprecise fashion. Though it is suspected that the mapping computed by this procedure does indeed takes small circles to small ellipses of bounded eccentricity, this has not been rigorously proven.

Though this algorithm is quite versatile and helpful for studying curvature flows, it is prudent to mention some challenges that have yet to be overcome. In particular, the implementation considered here can be somewhat sensitive to initial data due to the high degree of nonlinearity present in the p-Willmore equation, especially when large values of  $p$  are considered. Moreover, since the p-Willmore flow is not bounded from below when  $p$  is odd, poor behavior can also result if the energy becomes negative during the flow. Future work should elucidate ways in which both of these difficulties can be mitigated to produce a more robust p-Willmore flow model.

## 2. PRELIMINARIES

It is beneficial to recall how to manipulate evolving surfaces mathematically. Let  $\varepsilon > 0$  and  $u : M \times (-\varepsilon, \varepsilon) \rightarrow \mathbb{R}^3$  be a compactly supported family of surface immersions with images  $M(t) := u(M, t)$ , and let  $\delta := d/dt|_{t=0}$  denote the variational derivative operator. If  $\dot{u}$  denotes differentiation with respect to  $t$ , then the initial surface  $M(0)$  is said to undergo p-Willmore flow provided the equation

$$(3) \quad \dot{u} = -\delta \mathcal{W}^p,$$

is satisfied for all  $t$  in some interval  $(0, T]$ . Using standard techniques from the calculus of variations, it can be shown (see [1]) that for closed surfaces  $M$  this condition implies the scalar equation

$$(4) \quad \dot{u} \cdot N = \frac{p}{2} \Delta H^{p-1} + pH^{p-1}(2H^2 - K) - 2H^{p+1},$$

where  $N : M \times (-\varepsilon, \varepsilon) \rightarrow S^2$  is the inward-directed unit normal vector to  $M(t)$  for each  $t$ , and  $K$  is the Gauss curvature of the evolving surface.

**Remark 2.1.** Note that form here on the Einstein summation convention will be employed, so that any index appearing twice in an expression (once up and once down) will be implicitly traced over.

While equation (3) can be discretized by itself and used to define a normally-directed p-Willmore flow, it is advantageous to work directly with position instead of the mean curvature  $H$ . Besides being more

straightforward to implement, this allows for the consideration of tangential motion during the flow which can help regularize the surface mesh as it evolves (see [16]).

**Remark 2.2.** Though position-based flow techniques are more standard in the literature, researchers in [15] have had success working directly with curvature. Using a natural integrability condition, they are able to recover surface positions that maintain full conformality with respect to the reference immersion. A major advantage of this approach is that such conformality is built directly into the flow, completely eradicating mesh degradation along the evolution.

To develop a suitable model for the p-Willmore flow of surfaces, it is helpful to adopt the formalism of G. Dziuk found in [2]. To that end, let  $X : U \subset \mathbb{R}^2 \rightarrow M$  be a parametrization of (a portion of) the closed surface  $M$ , with inward-directed unit normal field  $N$ . Then, the identity map  $u : M \rightarrow \mathbb{R}^3$  defined through  $u \circ X = X$  provides an isometric surface immersion, and the components of the induced metric on  $M \subset \mathbb{R}^3$  are given by

$$(5) \quad g_{ij} = \partial_i X \cdot \partial_j X := X_i \cdot X_j.$$

With this, the surface gradient  $\nabla_M$  of a function  $f : M \rightarrow \mathbb{R}^3$  can be expressed componentwise as

$$(6) \quad (\nabla_M f) \circ X = g^{ij} X_i F_j,$$

where  $F = f \circ X$  is the pullback of  $f$  through the parametrization  $X$  and  $g^{ik} g_{kj} = \delta_j^i$ . It follows that the Laplace-Beltrami operator  $\Delta_M$  on  $M$  is then

$$(7) \quad (\Delta_M f) \circ X = (\nabla_M \cdot \nabla_M f) \circ X = \frac{1}{\sqrt{\det g}} \partial_j (\sqrt{\det g} g^{ij} F_i).$$

Moreover, in view of the geometric identity  $Y := \Delta_M u = 2HN$ , the p-Willmore functional is expressed succinctly in this framework as

$$(8) \quad \mathcal{W}^p(u) = \frac{1}{2^p} \int_M (Y \cdot N)^p.$$

**Remark 2.3.** Since the constant factor in front of the p-Willmore integrand merely scales the value of the functional and does not affect its geometric behavior, it will be omitted in subsequent passages with the understanding that  $\mathcal{W}^p$  truly indicates  $2^p \mathcal{W}^p$ . Note that this will manifest itself in the flow only as a uniform scaling of the time domain.



FIGURE 3. Volume-preserving 2-Willmore flow with mesh regularization applied to a genus 4 statue mesh.

### 3. BUILDING THE P-WILLMORE FLOW MODEL

It is now possible to calculate the variational derivative ( $L^2$ -gradient) of the functional  $\mathcal{W}^p$  in a way that is respectful with regards to computer implementation. More precisely, the calculation presented here involves no adapted coordinate system or explicit second-order derivatives, and the variations considered are assumed to have tangential as well as normal components. This will make it possible to accomplish the finite element discretization seen later.

Recall that when given a smooth function  $\varphi : M \rightarrow \mathbb{R}^3$  and a parameter  $t \in (-\epsilon, \epsilon)$ , a variation of  $u$  is given by

$$(9) \quad u(x, t) = u(x) + t\varphi(x),$$

where  $x$  denotes a local coordinate on  $M$ . This in turn induces a variation in the area functional, which can be calculated as in [2]. In particular, there is the following lemma from that work.

**Lemma 3.1.** *Let Greek letters indicate tensor components with respect to the standard basis for  $\mathbb{R}^3$ , and define  $D(\varphi)_{\alpha\beta} := (\nabla_M)_\alpha \varphi^\beta + (\nabla_M)_\beta \varphi^\alpha$ . Then, in the notation above and denoting the area functional on  $M$  by*

$$(10) \quad \mathcal{A}(u) = \int_M 1,$$

*the first and second variations of  $\mathcal{A}$  may be expressed as*

$$(11) \quad A'(u)(\varphi) = \int_M \nabla_M \cdot \varphi = \int_M \nabla_M u : \nabla_M \varphi,$$

$$(12) \quad \begin{aligned} A''(u)(\varphi, \psi) &= - \int_M (\nabla_M)_\beta \varphi^\alpha (\nabla_M)_\alpha \psi^\beta - N_\alpha N_\beta \nabla_M \varphi^\beta \cdot \nabla_M \psi^\alpha - \nabla_M \cdot \varphi \nabla_M \cdot \psi \\ &= - \int_M D(\varphi) \nabla_M u : \nabla_M \psi - \nabla_M \varphi : \nabla_M \psi - \nabla_M \cdot \varphi \nabla_M \cdot \psi. \end{aligned}$$

*Proof.* The proof is a direct calculation and can be found in [2].  $\square$

With this in place, it is helpful also to recall an operator splitting technique employed in [2] which is used to effectively reduce the order of the problem. In particular, let  $H^1(M)$  denote the Sobolev space of weakly first differentiable functions on  $M$  (note that compact support follows immediately since  $M$  is closed), and recall the equation  $Y = \nabla_M u$ . Integrating this by parts against  $\psi \in H^1(M)$  then yields the equation

$$(13) \quad \int_M Y \cdot \psi + \nabla_M u : \nabla_M \psi = 0,$$

which can be considered as a weak-form expression of the mean curvature vector  $Y$ . Note that due to the definition of  $Y$ , (13) has the useful function of effectively reducing the order of the p-Willmore flow equation (3) by 2 at the expense of solving an additional PDE.

It is now pertinent to develop a counterpart to equation (13), so that the operator splitting above can be beneficial. The resulting equation should reduce to (4) in the normal direction while also suppressing undesirable terms such as  $K$ . To accomplish this, it is beneficial to differentiate (13) implicitly with respect to  $t$ . Then, it follows that for an arbitrary  $\psi \in H^1(M)$ ,

$$(14) \quad \begin{aligned} 0 &= \int_M \delta Y \cdot \psi + (Y \cdot \psi) \nabla_M \cdot \varphi + A''(u)(\varphi, \psi) \\ &= \int_M \delta Y \cdot \psi + (Y \cdot \psi + \nabla_M \cdot \psi) \nabla_M \cdot \varphi + \nabla_M \psi : \nabla_M \varphi - D(\varphi) \nabla_M u : \nabla_M \psi, \end{aligned}$$

where Lemma 3.1 was used in the last equality. The goal is now to use this expression to develop a weak-form for the p-Willmore equation by choosing an appropriate test function. In addition, this choice should be made in avoidance of explicit derivatives of the normal vector  $N$ , since they are not well-suited to discretization using piecewise-linear finite elements. To this end, note that the squared norm of  $Y$  can be expressed as

$$(15) \quad |Y|^2 = (Y \cdot N)^2,$$

so that after differentiating both sides with respect to  $t$ , there is the relationship

$$(16) \quad \delta Y \cdot Y = (Y \cdot N) \delta(Y \cdot N).$$

Using this, it follows that the derivative of the p-Willmore integrand  $(Y \cdot N)^p$  may be expressed as follows

$$(17) \quad \delta(Y \cdot N)^p = p(Y \cdot N)^{p-1} \delta(Y \cdot N) = p(Y \cdot N)^{p-2} (\delta Y \cdot Y) = \delta Y \cdot (p(Y \cdot N)^{p-2} Y).$$

Hence, letting  $W := (Y \cdot N)^{p-2}Y$  be the weighted mean curvature vector on  $M$  and choosing  $\psi = pW$  in equation (14), the variation of the ( $2^p$ -scaled) Willmore functional  $\mathcal{W}^p$  can be calculated as

$$(18) \quad \begin{aligned} \delta\mathcal{W}^p(u) &= \delta \int_M (Y \cdot N)^p = \int_M p(\delta Y \cdot (Y \cdot N)^{p-2}Y) + \int_M (Y \cdot N)^p \nabla_M \cdot \varphi \\ &= \int_M ((1-p)(Y \cdot N)^p - p\nabla_M \cdot W) \nabla_M \cdot \varphi + p((D(\varphi)\nabla_M u - \nabla_M \varphi) : \nabla_M W). \end{aligned}$$

This directly implies the following Theorem.

**Theorem 3.2.** *In the notation above and for  $p \geq 1$ , the  $p$ -Willmore flow equation (3) is expressed in weak form by the following system of PDE in the variables  $u$ ,  $Y$ , and  $W$ :*

$$(19) \quad \begin{aligned} &\int_M \dot{u} \cdot \varphi + ((1-p)(Y \cdot N)^p - p\nabla_M \cdot W) \nabla_M \cdot \varphi \\ &\quad + pD(\varphi)\nabla_M u : \nabla_M W - p\nabla_M \varphi : \nabla_M W = 0, \end{aligned}$$

$$(20) \quad \int_M Y \cdot \psi + \nabla_M u : \nabla_M \psi = 0,$$

$$(21) \quad \int_M W \cdot \xi - (Y \cdot N)^{p-2}Y \cdot \xi = 0,$$

which must hold for all  $t \in (0, T]$  and all  $\varphi, \psi, \xi \in H^1(M(t))$ .

*Proof.* The proof follows immediately from the definitions of  $Y, W$ , and the discussion above.  $\square$

**Remark 3.3.** The reader will notice that this reduces to precisely the system in [2] for the case  $p = 2$ , in which case the last equation is not needed. Additionally, the case  $p = 0$  (mean curvature flow)—while not in the domain of the theorem as stated—may be recovered by simply omitting (21) and replacing equation (19) with the equation from Lemma 3.1 for the variation of area:

$$(22) \quad \int_M \dot{u} \cdot \varphi - \nabla_M u : \nabla_M \varphi = 0.$$

The system in Theorem 3.2 is the primary model for the  $p$ -Willmore flow studied here, and provides the basis for the  $p$ -Willmore flow algorithm presented later. Note that it provides a unified framework in which to study several important curvature flows including MCF, GCF, and the Willmore flow. Before discussing further modifications to this model, the following theoretical result is presented which guarantees that the  $p$ -Willmore energy always decreases along the flow governed by the equations above. An example illustration is given in Figure 4.

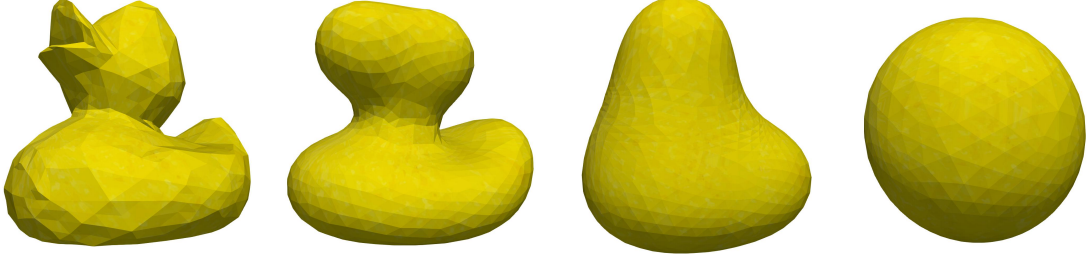


FIGURE 4. The 2-Willmore flow applied to a rubber duck mesh. Note the convergence to a round sphere, illustrating the energy decreasing property of the flow.

**Theorem 3.4.** *The closed surface  $p$ -Willmore flow is energy decreasing for  $p \geq 1$ . That is, if  $W = (Y \cdot N)^{p-2}Y$  is the weighted mean curvature vector on  $M$  and  $u : M \times (0, T] \rightarrow \mathbb{R}^3$  is family of surface immersions with  $M(t) = u(U, t)$  satisfying the weak  $p$ -Willmore flow equations*

$$(23) \quad \int_M \dot{u} \cdot \varphi + (1-p)(Y \cdot N)^p \nabla_M \cdot \varphi - p(\nabla_M \cdot W) \nabla_M \cdot \varphi$$

$$(24) \quad + pD(\varphi) \nabla_M u : \nabla_M W - p \nabla_M W : \nabla_M \varphi = 0,$$

$$(25) \quad \int_M Y \cdot \psi + \nabla_M u : \nabla_M \psi = 0,$$

$$(26) \quad \int_M W \cdot \xi - (Y \cdot N)^{p-2}Y \cdot \xi = 0,$$

then the  $p$ -Willmore flow satisfies

$$(27) \quad \int_{M(t)} |\dot{u}|^2 + \frac{d}{dt} \int_{M(t)} (Y \cdot N)^p = 0.$$

**Remark 3.5.** This property is well-known in the case of MCF (0-Willmore flow), so the proof of this case is omitted. See e.g. [27] for more details.

*Proof.* Recall that differentiation of (13) yields

$$(28) \quad \int_M \delta Y \cdot \psi + (Y \cdot \psi + \nabla_M \cdot \psi) \nabla_M \cdot \varphi + \nabla_M \psi : \nabla_M \varphi - D(\varphi) \nabla_M u : \nabla_M \psi = 0.$$

Choosing the admissible test functions  $\varphi = \dot{u}$  and  $\psi = pW$ , and noticing that  $W \cdot Y = (Y \cdot N)^p$ , the following system is observed

$$(29) \quad \int_M |\dot{u}|^2 + (1-p)(Y \cdot N)^p \nabla_M \cdot \dot{u} - p(\nabla_M \cdot W) \nabla_M \cdot \dot{u} + pD(\dot{u}) \nabla_M u : \nabla_M W - p \nabla_M W : \nabla_M \dot{u} = 0,$$

$$(30) \quad \int_M p(\delta Y \cdot W) + p((Y \cdot N)^p + \nabla_M \cdot W) \nabla_M \cdot \dot{u} + p \nabla_M W : \nabla_M \dot{u} - pD(\dot{u}) \nabla_M u : \nabla_M W = 0.$$

Noting (17) and adding the above equations then yields

$$(31) \quad \int_M |\dot{u}|^2 + \delta(Y \cdot N)^p + (Y \cdot N)^p \nabla_M \cdot \dot{u} = \int_M |\dot{u}|^2 + \frac{d}{dt} \int_M (Y \cdot N)^p = 0,$$

completing the argument.  $\square$

Now, in light of the physical relevance of the functional  $\mathcal{W}^p$ , it is desirable also to have a model for the p-Willmore flow that is amenable to geometric constraints on surface area and enclosed volume. This is reasonable not only from a physical point of view (since many curvature-minimizing structures such as biomembranes constrain themselves naturally in these ways) but also in a mathematical sense, as such constraints can serve as a meaningful ‘‘replacement’’ for conformal invariance when  $p \neq 2$ . More precisely, since the p-Willmore functional is not conformally invariant in general, volume/area preservation ensures that physically-meaningful shapes such as spheres remain locally minimizing for  $p \neq 2$ , at least among some class of variations. Practically, this is accomplished through the addition of Lagrange multipliers  $\lambda, \mu$  into the model from Theorem 3.2. More precisely, let  $D \subset \mathbb{R}^3$  be a region in space such that  $\partial D = M$  and recall the volume functional,

$$(32) \quad \mathcal{V} = \int_D 1 = \frac{1}{3} \int_D \nabla \cdot u = \frac{1}{3} \int_M u \cdot N,$$

where the divergence theorem was applied in the last equality. It is well-known (see e.g. [28]) that the first variation of volume is given by

$$(33) \quad \delta\mathcal{V} = \int_M \varphi \cdot N.$$

On the other hand, recall that Lemma 3.1 implies that the first variation of the area functional can be expressed as

$$(34) \quad \delta\mathcal{A} = \delta \int_M 1 = \int_M \nabla_M u : \nabla_M \varphi.$$

With these expressions available, it is straightforward to define the next problem considered in this work: closed surface p-Willmore flow with constraint.

**Problem 3.6** (Closed surface p-Willmore flow with constraint). *Let  $p \geq 1$  and  $W := (Y \cdot N)^{p-2} Y$ . Determine a family  $u : M \times (0, T] \rightarrow \mathbb{R}^3$  of immersions with  $M(t) := u(M, t)$  such that  $M(0)$  has initial volume  $V_0$ , initial surface area  $A_0$ , and the equation*

$$(35) \quad \dot{u} = \delta (\mathcal{W}^p + \lambda\mathcal{V} + \mu\mathcal{A}),$$

is satisfied for some piecewise-constant functions  $\lambda, \mu$  and for all  $t \in (0, T]$ . Stated in weak form, the goal is to find functions  $u, Y, W, \lambda, \mu$  on  $M(t)$  such that the equations

$$(36) \quad \int_M \dot{u} \cdot \varphi + \lambda(\varphi \cdot N) + \mu \nabla_M u : \nabla_M \varphi + ((1-p)(Y \cdot N)^p - p \nabla_M \cdot W) \nabla_M \cdot \varphi \\ + p D(\varphi) \nabla_M u : \nabla_M W - p \nabla_M \varphi : \nabla_M W = 0,$$

$$(37) \quad \int_M Y \cdot \psi + \nabla_M u : \nabla_M \psi = 0,$$

$$(38) \quad \int_M W \cdot \xi - (Y \cdot N)^{p-2} Y \cdot \xi = 0,$$

$$(39) \quad \int_M 1 = A_0,$$

$$(40) \quad \int_M u \cdot N = 3V_0,$$

are satisfied for all  $t \in (0, T]$  and all  $\varphi, \psi, \xi \in H^1(M(t))$ .

**Remark 3.7.** The case where  $p = 0$  may again be considered by replacing the equation (36) with the simpler relationship

$$(41) \quad \int_M \dot{u} \cdot \varphi + \lambda(\varphi \cdot N) - \nabla_M u : \nabla_M \varphi = 0.$$

Note that area preservation makes no sense in this context (since the objective of MCF is to decrease area), so equation (39) should also be disregarded in this case.

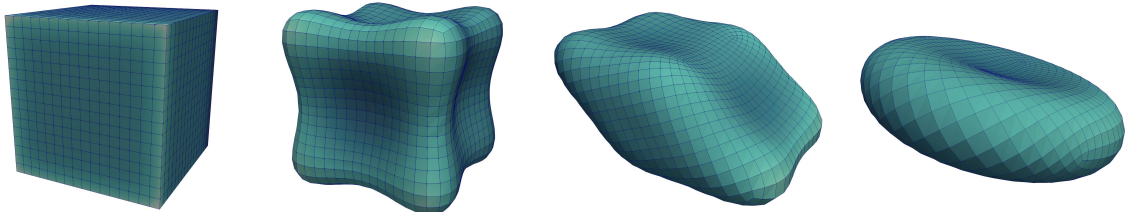


FIGURE 5. Willmore evolution of a cube, constrained by both surface area and enclosed volume. Here appears the biconcave discoid shape characteristic of genus 0 minimizers of the constrained Helfrich energy such as red blood cells [29]. It is further remarkable that the flow behavior here is different than when either constraint is considered on its own, where the cube becomes a round sphere instead.

Problem 3.6 provides a way to examine the p-Willmore flow subject to geometric constraints on surface area or enclosed volume. This is a highly interesting situation, since minimizing surfaces can vary wildly with the type of constraint that is considered. For example, when beginning with the surface of a cube,

enforcing either volume or area preservation separately produces a spherical minimizer. On the other hand, Figure 5 displays the behavior of a cube under 2-Willmore flow when constrained by both surface area and enclosed volume together. This scenario arises frequently in mathematical biology when considering membrane behavior in an external solution, and minimizing surfaces often realize familiar shapes such as the biconcave discoid typical of red blood cells. See [29] for further details.

**Remark 3.8.** Note that the system in Problem 3.6 can also be used to study the p-Willmore flow with fixed volume or fixed surface area separately. In particular, fixed volume is obtained by setting  $\mu \equiv 0$  and ignoring (39), and fixed area is accomplished similarly with  $\lambda \equiv 0$  and omission of (40). In practice, Boolean variables were implemented to enable switching between the different constrained/unconstrained cases.

#### 4. BUILDING THE MESH REGULARIZATION EQUATIONS

One of the main questions that arises in the computer implementation of curvature flows is how to preserve the quality of the surface mesh as it evolves. If the initial mesh becomes sufficiently degenerate along the flow, it will crash the simulation—sometimes well before any troublesome behavior occurs in the actual surface geometry (see Figure 7). Since curvature flows often alter the initial surface quite dramatically, this can present a serious issue for accurately modeling flow behavior. Several different techniques have been developed to combat this issue e.g. [30, 25, 31, 32, 33], each with their own strengths and weaknesses. A common challenge present in all methods of mesh regularization is striking a good balance between area-preservation and conformality, or angle-preservation. Of course, area-preserving maps can be arbitrarily ugly (think following the flow of a vector field on the surface) and conformal maps frequently distort area in undesirable ways. Therefore, the technique employed in this work is inspired by the least-squares conformal mapping procedure of [25] as well as the following result from [3], which can be thought of as a generalization of the Cauchy-Riemann equations from classical complex analysis.

**Theorem 4.1.** (*Kamberov, Pedit, Pinkall*) *Let  $X : M \rightarrow \text{Im}\mathbb{H}$  be an immersion of  $M$  into the imaginary part of the quaternions, and let  $J$  be a complex structure (rotation operator  $J^2 = -\text{Id}_{TM}$ ) on  $TM$ . Then, if  $*\alpha = \alpha \circ J$  is the usual Hodge star on differential forms, it follows that  $X$  is conformal if and only if there is a Gauss map (unit normal field)  $N : M \rightarrow \text{Im}\mathbb{H}$  such that  $*dX = N dX$ .*

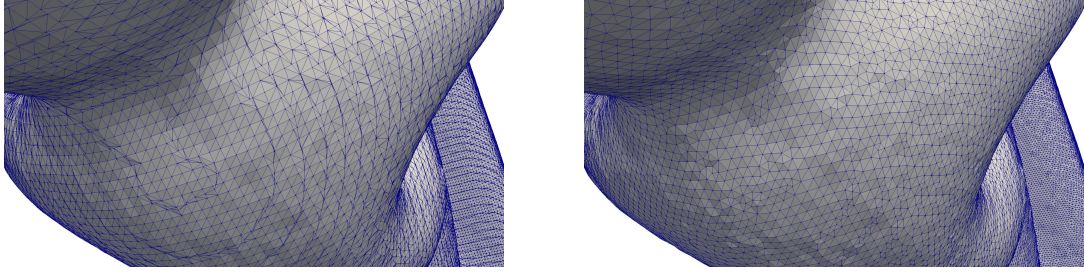


FIGURE 6. The mesh regularization procedure described in Problem 4.3 applied to a statue mesh, with close-up on the back of one figure. Before (left) and after (right). Notice the large improvement in triangle quality that results from the minimization.

Since  $\text{Im } \mathbb{H}$  is canonically isomorphic to  $\mathbb{R}^3$  as a vector space, this gives a criterion for conformality that can be weakly enforced during the p-Willmore flow. More precisely, recall that  $N \perp dX(v)$  for all tangent vectors  $v \in TM$ , and that multiplication of  $v, w \in \text{Im } \mathbb{H}$  obeys the rule  $vw = -v \cdot w + v \times w$ . It follows that  $N dX(v) = N \times dX(v)$  for all  $v \in TM$ , and the conformality condition in Theorem 4.1 can be expressed weakly as

$$(42) \quad * dX(v) = N \times dX(v) \quad \text{for all } v \in TM.$$

For the present purpose of mesh regularization, it suffices to enforce this condition implicitly through a minimization procedure. Define the conformal distortion functional

$$(43) \quad \mathcal{CD}(u) = \frac{1}{2} \int_M |\nabla_{Jv} u - N \times \nabla_v u|^2,$$

where  $\nabla_v u = du(v)$  is the derivative of  $u$  in the direction  $v$ . Minimization of this functional leads to the necessary condition

$$(44) \quad \delta \mathcal{CD} = \int_M (\nabla_{Jv} u - N \times \nabla_v u) \cdot (\nabla_{Jv} \varphi - N \times \nabla_v \varphi) = 0,$$

for all  $v \in TM$ . Since this is a linear condition, it can be enforced on a basis  $e_1, e_2$  for  $TM$ , leading to the equation

$$(45) \quad \begin{aligned} & \int_M (\nabla_{M,2} u - N \times \nabla_{M,1} u) \cdot (\nabla_{M,2} \varphi - N \times \nabla_{M,1} \varphi) \\ & + \int_M (\nabla_{M,1} u + N \times \nabla_{M,2} u) \cdot (\nabla_{M,1} \varphi + N \times \nabla_{M,2} \varphi) = 0, \end{aligned}$$

where  $\nabla_{M,i} := (\nabla u - (\nabla u \cdot N)N) \cdot e_i$  and  $\nabla$  is the usual flat derivative on  $\mathbb{R}^3$ .

**Remark 4.2.** For implementation purposes, these calculations are done by pulling the surface back (locally) to  $U$  through the parametrization  $X$ , where there is a natural orthonormal basis given by  $\{\partial/\partial x^1, \partial/\partial x^2\}$  for the usual Cartesian coordinates  $(x^1, x^2)$  coordinates on  $U$ . Since  $u \circ X = X$ , this is trivially accomplished in practice, as the surface derivatives become simply  $\nabla_{M,i} u = \partial X / \partial x^i$ .

Of course, if the above equation is to be useful as an effective reparametrization of surface evolving by p-Willmore flow, it should not be solved arbitrarily. (In particular, it is clear that any constant function will satisfy the equation as stated.) So, it is necessary to develop also a condition which ensures that this mesh regularization does not destroy the current surface geometry. One such condition is motivated by the following observation: if the aim is to recover new positions  $u$  which lie on the same geometric surface as the current data  $\tilde{u}$ , then (to first order) the difference  $u_h - \tilde{u}_h$  should be orthogonal to the surface normal  $N$ . Said differently, a first-order approximation to tangential motion can be enforced by requiring the equation

$$(46) \quad \int_M (\tilde{u} - u) \cdot N = 0,$$

to hold during the above minimization. Specifically, the quasi-conformal mesh regularization procedure is presented as the following problem.

**Problem 4.3** (quasi-conformal mesh regularization). *Given surface positions  $\tilde{u}$ , solving the quasi-conformal mesh regularization problem amounts to finding new positions  $u$  and a Lagrange multiplier  $\rho$  which satisfy the system*

$$(47) \quad \begin{aligned} & \int_M \rho(\varphi \cdot N) + (\nabla_{M,2} u - N \times \nabla_{M,1} u) \cdot (\nabla_{M,2} \varphi - N \times \nabla_{M,1} \varphi) \\ & + (\nabla_{M,1} u + N \times \nabla_{M,2} u) \cdot (\nabla_{M,1} \varphi + N \times \nabla_{M,2} \varphi) = 0, \end{aligned}$$

$$(48) \quad \int_M (u - \tilde{u}) \cdot N = 0.$$

Solving Problem 4.3 at each step of the p-Willmore flow inhibits the computer simulation from breaking arbitrarily, at the expense of first-order accuracy in the flow. To be sure, without such a procedure in place it is not unusual for global minimizers to remain computationally out-of-reach, as is shown in Figure 7. Moreover, Figure 6 demonstrates how this regularization is useful even for stationary surfaces, as it greatly improves the quality of (even very irregular) surface meshes. The practical discretization of both this system and the p-Willmore system in Problem 3.6 will be discussed in the next sections.

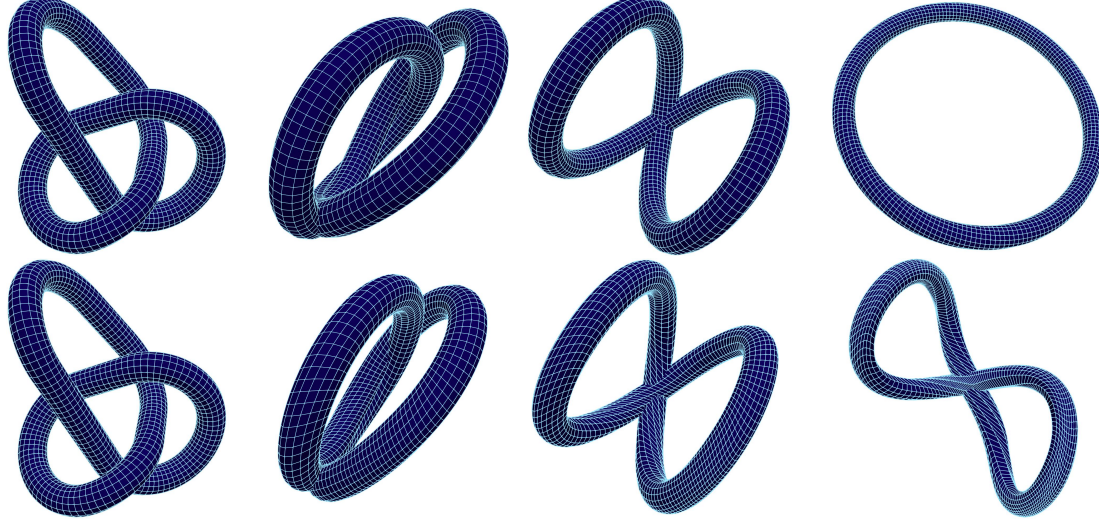


FIGURE 7. Surface area and volume constrained 2-Willmore evolution of a trefoil knot, with conformal mesh regularization (top) and without (bottom). Notice that the mesh degrades when not regularized, preventing movement to the minimizing surface. Conversely, the mesh quality remains nearly perfect along the flow when regularized at each step, and evolves completely to the desired minimum.

## 5. DISCRETIZATION OF MODEL SYSTEMS

Discretization of the models in Problem 3.6 and Problem 4.3 will now be discussed. In particular, specifics of the spatial discretization will be presented, and it will be demonstrated in the style of [2, 16] that (under some assumptions) the discretization of the p-Willmore flow system in Theorem 3.2 is numerically stable. Further, it will be shown that the discrete model is consistent with its continuous counterpart in the sense that the error between the continuous and discrete p-Willmore energies goes to zero with the parameter stepsize.

To that end, as in [16] the smooth surface  $M \subset \mathbb{R}^3$  is approximated by a polygonal surface  $M_h$  consisting of 2-simplices (triangles)  $T_h$  that are not degenerate, so that

$$(49) \quad M_h = \bigcup_{T_h \in \mathcal{T}_h} T_h,$$

forms a triangulation of  $M$ . Denoting the nodes of this triangulation by  $\{a_j\}_{j=1}^N$ , the standard nodal basis  $\{\phi_i\}$  satisfies  $\phi_i(a_j, t) = \delta_{ij}$ . The space of piecewise-linear finite elements on  $M_h(t)$  is then

$$(50) \quad S_h(t) = \text{Span}\{\phi_i\} = \{\phi \in C^0(M_h(t)) : \phi|_{T_h} \in \mathbb{P}_1(T_h), T_h \in \mathcal{T}_h\}.$$

Now, suppose the simplices  $T_h \in \mathcal{T}_h$  have maximum diameter  $h$  with inner radius bounded from below by  $ch$  for some  $c > 0$ . Then, for any choice of unit normal  $N$  there is  $\delta > 0$  so that points  $x \in \mathbb{R}^3$  in the tube of radius delta around  $M$  can be expressed as

$$(51) \quad x = a(x) + d(x)N(x),$$

where  $a(x)$  lies on  $M$  and  $|d| < \delta$ . It is assumed that  $M_h$  is contained in this tube, so that any function  $f_h$  defined on the discrete surface  $M_h$  can be lifted to a function  $f_h^l$  on the smooth surface  $M$  by requiring

$$(52) \quad f_h^l(a(x)) = f_h(x), \quad x \in M_h.$$

Denote the inverse process by  $f^{-l}$ . In this notation, the lift of the finite element space  $S_h$  is denoted

$$(53) \quad S_h^l = \{\phi^l \mid \phi \in S_h\},$$

and it is possible to compare geometric quantities on  $M$  and  $M_h$ . In particular, the following Proposition is amalgamated from results in [2].

**Proposition 5.1.** *In the notation above, and assuming that the nodes  $a_j$  lie on the surface  $M$ , the following estimates hold:*

(a) *The distance between the surfaces  $M(t)$  and  $M_h(t)$  satisfies*

$$(54) \quad \|d(\cdot, t)\|_{L^\infty(M_h)} \leq ch^2.$$

(b) *The quotient  $\delta_h$  between the smooth and discrete surface measures, satisfying  $\delta_h dA_h = dA$ , satisfies*

$$(55) \quad \sup_{M_h} |1 - \delta_h| \leq ch^2.$$

(c) *For any function  $f \in H^2(M)$ , there is an interpolation operator  $I_h$  such that  $I_h f \in S_h^l$  satisfies*

$$(56) \quad \|f - I_h f\|_{L^2(M)} + h \|\nabla_M(f - I_h f)\|_{L^2(M)} \leq ch^2 \|f\|_{H^2(M)}.$$

(d) *Let  $Y_h = \Delta_{M_h} u_h$  be the discrete mean curvature vector satisfying*

$$(57) \quad \int_{M_h} Y_h \cdot \psi_h + \nabla_{M_h} u_h : \nabla_{M_h} \psi_h = 0, \quad \forall \psi_h \in S_h.$$

*Then, its lift  $Y_h^l$  satisfies the estimate*

$$(58) \quad \|Y - Y_h^l\|_{L^2(M)} \leq ch(1 + \|Y\|_{H^2}).$$

(e) For all  $\psi_h \in S_h$ ,

$$(59) \quad \int_M (Y - Y_h^l) \cdot \psi_h^l \leq ch^2 \int_M |\nabla_M \psi_h^l| + ch^2 \int_M |Y_h^l| |\psi_h^l|.$$

*Proof.* See [2]. In particular, Lemmas 6.1, 6.2, and Theorem 6.3.  $\square$

With these estimates established, it is possible to state the discrete p-Willmore flow equations. It will be useful to require that

$$(60) \quad \int_{M_h} u_h = \int_{M_h} u^{-l},$$

(which can be accomplished using an appropriate Ritz projection) so that integration can be performed over the discrete surface  $M_h$  as opposed to  $M$ . The discrete  $p$ -Willmore functional is then given as

$$(61) \quad \mathcal{W}^p(u_h) = \frac{1}{2^p} \int_{M_h} (Y_h \cdot N_h)^p,$$

and the discrete p-Willmore flow problem can be stated as follows.

**Problem 5.1** (Discrete unconstrained p-Willmore flow). *Given  $p \geq 1$  and  $M_h(0)$  a nondegenerate triangulated surface with maximum diameter  $h > 0$ , find a family  $X_h(t)$  of immersions with images  $M_h(t)$  and identity maps  $u_h(X_h, t)$  satisfying*

$$(62) \quad \dot{u}_h = -\delta \mathcal{W}^p(u_h),$$

for all  $t \in (0, T]$ . In weak form, given the discrete inner unit normal  $N_h$ , find functions  $u_h$  and  $W_h := (Y_h \cdot N_h)^{p-2} Y_h$

$$(63) \quad \begin{aligned} & \int_{M_h} \dot{u}_h \cdot \varphi_h + ((1-p)(Y_h \cdot N_h)^p - p \nabla_{M_h} \cdot W_h) \nabla_{M_h} \cdot \varphi_h \\ & + p((D_h(\varphi_h) \nabla_{M_h} u_h - \nabla_{M_h} \varphi_h) : \nabla_{M_h} W_h) = 0, \end{aligned}$$

$$(64) \quad \int_{M_h} Y_h \cdot \psi_h + \nabla_{M_h} u_h : \nabla_{M_h} \psi_h = 0,$$

$$(65) \quad \int_{M_h} W_h \cdot \xi_h - (Y_h \cdot N_h)^{p-2} Y_h \cdot \xi_h = 0,$$

for all  $\varphi_h, \psi_h, \xi_h \in H^1(M_h(t))$ .

*Proof.* This discrete formulation follows immediately from Theorem 3.2 and the discussion above.  $\square$

It is now prudent to check that the function  $u_h$  obtained as a solution to Problem 5.1 is consistent with the theoretical solution  $u$  to Problem 3.6 when  $\lambda, \mu \equiv 0$ . In other words, it should be verified that the error

between the continuous and discrete solutions goes to zero with the stepsize in some suitable norm. To that end, the following result is presented.

**Proposition 5.2.** *Suppose  $u_h \in S_h$  is a solution of*

$$(66) \quad \int_{M_h} \nabla_{M_h} u_h : \nabla_{M_h} \psi_h = \int_{M_h} \nabla_{M_h} u^{-l} : \nabla_{M_h} \psi_h, \quad \forall \psi_h \in S_h,$$

*and  $|Y|$  is uniformly bounded on  $M$ . Then, for some constant  $c \in \mathbb{R}$  the difference between the continuous and discrete  $p$ -Willmore energy satisfies*

$$(67) \quad |\mathcal{W}^p(u) - \mathcal{W}^p(u_h)| \leq ch^2.$$

*Proof.* The argument is adapted from [2]. First, the estimate between the discrete and continuous surface measures implies

$$(68) \quad \begin{aligned} 2^p |\mathcal{W}^p(u) - \mathcal{W}^p(u_h)| &\leq \left| \int_M |Y|^p - \int_{M_h} |Y_h|^p \right| = \left| \int_M |Y|^p - \int_M |Y_h^l|^p \frac{1}{\delta_h} \right| \\ &\leq \int_M ||Y|^p - |Y_h^l|^p| + \int_M |Y_h^l|^p \left| 1 - \frac{1}{\delta_h} \right|. \end{aligned}$$

Further, by writing  $|\cdot|^p = (|\cdot|^2)^{p/2}$ , the Mean Value Theorem applied to  $f(x) = |x|^{p/2}$  implies there is  $\zeta$  satisfying (note that  $M$  is compact)

$$(69) \quad \min_M \{|Y|^2, |Y_h^l|^2\} \leq \zeta \leq \max_M \{|Y|^2, |Y_h^l|^2\},$$

which satisfies the equality

$$(70) \quad ||Y|^p - |Y_h^l|^p| = \frac{p}{2} |\zeta|^{\frac{p-2}{2}} ||Y|^2 - |Y_h^l|^2|.$$

Using this, the estimate from above can be continued as

$$(71) \quad \begin{aligned} &\int_M ||Y|^p - |Y_h^l|^p| + \int_M |Y_h^l|^p \left| 1 - \frac{1}{\delta_h} \right| = \frac{p}{2} \int_M |\zeta|^{\frac{p-2}{2}} ||Y|^2 - |Y_h^l|^2| + \int_M |Y_h^l|^p \left| 1 - \frac{1}{\delta_h} \right| \\ &\leq \frac{p}{2} \int_M |\zeta|^{\frac{p-2}{2}} |(Y - Y_h^l) \cdot (Y + I_h Y - I_h Y + Y_h^l)| + ch^2 \int_M |Y_h^l|^p \\ &\leq \frac{p}{2} \|Y\|_{L^\infty}^{\frac{p}{2}-1} \int_M |Y - I_h Y| |Y - Y_h^l| + |(I_h Y + Y_h^l) \cdot (Y - Y_h^l)| + ch^2 \int_M |Y_h^l|^p \\ &\leq \frac{p}{2} \|Y\|_{L^\infty}^{\frac{p}{2}-1} \|Y - I_h Y\|_{L^2} \|Y - Y_h^l\|_{L^2} + \frac{p}{2} \|Y\|_{L^\infty}^{\frac{p}{2}-1} \int_M |(I_h Y + Y_h^l) \cdot (Y - Y_h^l)| \\ &\quad + ch^2 \int_M |Y_h^l|^p, \end{aligned}$$

where uniform boundedness of  $|Y|$  was used and the last equality follows from Cauchy-Schwarz. Further, using Proposition 5.1,

$$(72) \quad \begin{aligned} \int_M |(Y - Y_h^l) \cdot (I_h Y + Y_h^l)| &\leq ch^2 \int_M |\nabla_M(I_h Y + Y_h^l)| + ch^2 \int_M |Y_h^l| |I_h Y + Y_h^l| \\ &\leq ch^2 (\|\nabla_M(I_h Y)\|_{L^1} + \|\nabla_M(Y_h^l)\|_{L^1} + \|I_h Y\|_{L^2}^2 + \|Y_h^l\|_{L^2}^2). \end{aligned}$$

Standard estimates (see [2]) now imply that the difference between the continuous and discrete p-Willmore energies satisfies

$$(73) \quad \begin{aligned} |\mathcal{W}^p(u) - \mathcal{W}^p(u_h)| &\leq c \|Y - I_h Y\|_{L^2} \|Y - Y_h^l\|_{L^2} \\ &+ ch^2 (\|\nabla_M(I_h Y)\|_{L^1} + \|\nabla_M(Y_h^l)\|_{L^1} + \|I_h Y\|_{L^2}^2 + \|Y_h^l\|_{L^2}^2) \\ &\leq ch^2 (1 + \|Y\|_{H^2}^2), \end{aligned}$$

as desired.  $\square$

Importantly, it is further possible to demonstrate the stability of the discrete p-Willmore flow Problem 5.1 when the exponent  $p$  is even. Indeed, it follows almost immediately from Theorem 3.4 that the numerical solution remains bounded along the flow in the appropriate norms.

**Proposition 5.3.** *Suppose  $p$  is even,  $u_h \in S_h$  is a solution of Problem 5.1 with initial value  $u_{h0} := u_h(\cdot, 0)$ , and denote  $M_{h0} := M_h(0)$ . Then, it follows that  $(Y_h \cdot N_h)^p = \|Y_h\|^p$ , and*

$$(74) \quad \int_{M_h} |\dot{u}_h|^2 + \frac{d}{dt} \int_{M_h} |Y_h|^p = 0.$$

Further, suppose  $u_{h0}$  is chosen so that (c.f. [2])

$$(75) \quad \sup_{\varphi_h \in S_h(0)} \|\varphi_h\|_{L^2(M_{h0})}^{-1} \int_{M_{h0}} \nabla_{M_{h0}} u_{h0} : \nabla_{M_{h0}} \varphi_h \leq c \|u_0\|_{H^2(M_0)},$$

where  $u_0$  is corresponding initial data for the continuous Problem 3.6. Then, the p-Willmore flow is numerically stable. In particular, it satisfies the inequality

$$(76) \quad \int_0^T \|\dot{u}_h\|_{L^2(M_h)}^2 dt + \sup_{t \in (0, T)} \|Y_h\|_{L^p(M_h)}^p \leq c \|u_0\|_{H^2(M_0)} \|W_h(\cdot, 0)\|_{L^2(M_0)}.$$

*Proof.* Note that integration by parts was not performed during the formulation of the continuous system in Theorem 3.2, and that the variation  $\varphi$  was never assumed to be totally normal to the surface. Therefore, using  $(\cdot, \cdot)$  to denote the  $L^2$  inner product, the equation (63) is equivalent to

$$(77) \quad (\dot{u}_h, \varphi_h)_{L^2(M_h)} + (\delta \mathcal{W}^p(u_h), \varphi_h)_{L^2(M_h)} = 0,$$

since the relevant variational calculations carry over without change to the spatially discrete setting. In light of this, equation (74) follows immediately from Theorem 3.4. To show the claimed inequality (76), it suffices to integrate the above equation with respect to  $t$ , in which case one sees

$$(78) \quad \int_0^t \|\dot{u}_h\|_{L^2(M_h)}^2 dt + \|Y_h(\cdot, t)\|_{L^p(M_h)}^p = \|Y_h(\cdot, 0)\|_{L^p(M_{h0})}^p$$

The term on the right hand side can now be estimated using the hypothesis and equation (13). Choosing the test function  $\varphi_h = W_h$ , it follows that

$$(79) \quad \|Y_h(\cdot, 0)\|_{L^p(M_{h0})}^p = - \int_{M_{h0}} \nabla_{M_{h0}} u_{h0} : \nabla_{M_{h0}} W_h(\cdot, 0) \leq c \|u_0\|_{H^2(M_0)} \|W_h(\cdot, 0)\|_{L^2(M_{h0})}.$$

Using this in (78) and noting that the resulting inequality holds for all  $t \in (0, T]$  then proves the final claim.  $\square$

**Remark 5.2.** When  $p$  is odd, the situation is more delicate. In this case, it can (and occasionally does) happen that the p-Willmore energy is negative during the flow. Since there is no global lower bound, this creates an unstable evolution which quickly breaks the simulation. On the other hand, if the flow encounters a positive minimum before the mean curvature becomes negative, it may still stabilize without issue. See see Figure 8 for an illustration of this phenomenon.

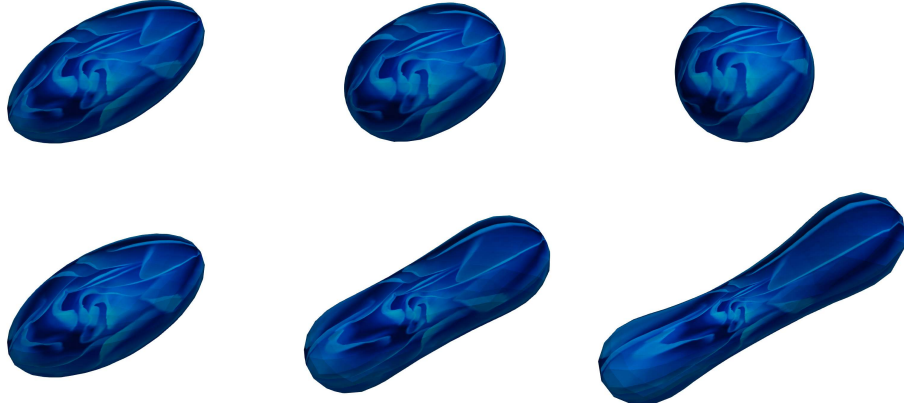


FIGURE 8. 3-Willmore flow applied to an ellipsoid with inward normal (top) and outward normal (bottom). Note that the mean curvature is pointwise negative when the outward normal is chosen, so the flow does not converge.

**Remark 5.3.** It is also remarkable that the norms employed in the above stability estimate are natural for the p-Willmore flow. In particular,  $Y$  is bounded with respect to  $L^p$ , which is meaningful since the p-Willmore energy  $\mathcal{W}^p$  can be considered as measuring the signed  $L^p$  norm of the mean curvature  $H$ .

Propositions 5.2 and 5.3 demonstrate the consistency and stability of the discretized p-Willmore flow system in Problem 5.1. Now that these issues have been discussed, it is appropriate to discuss the temporal discretization of the p-Willmore flow and mesh regularization systems, and give the full algorithm for running the closed surface p-Willmore flow with quasi-conformal mesh regularization.

## 6. ALGORITHM AND IMPLEMENTATION

It is finally appropriate to present the full algorithm for running the p-Willmore flow with quasi-conformal mesh regularization. This algorithm is completely automated in the sense that no user input is required after the initial specification of a surface mesh and parameter configuration. To accomplish this, the temporal discretization is now described. Let  $\tau > 0$  be a fixed temporal stepsize, and denote  $u_h^k := u_h(\cdot, k\tau)$ . To implement the p-Willmore flow Problem 3.6 beginning from the  $k^{th}$  time step where  $0 \leq k \leq T/\tau$ , the goal is to find  $\{\tilde{u}_h^{k+1}, \tilde{Y}_h^{k+1}, \tilde{W}_h^{k+1}, \lambda_h^{k+1}, \mu_h^{k+1}\}$  satisfying the system of equations

$$\begin{aligned} & \int_{M_h^k} \frac{(\tilde{u}_h^{k+1} - u_h^k)}{\tau} \cdot \varphi_h + \lambda_h^{k+1} (\varphi_h \cdot N_h^k) + \mu_h^{k+1} \nabla_{M_h^k} u_h^k : \nabla_{M_h^k} \varphi_h + (1-p)(\tilde{Y}_h^{k+1} \cdot N_h^k)^p \nabla_{M_h^k} \cdot \varphi_h \\ (80) \quad & - p(\nabla_{M_h^k} \cdot \tilde{W}_h^{k+1}) \nabla_{M_h^k} \cdot \varphi_h + p(D_h^k(\varphi_h) \nabla_{M_h^k} u_h^k - \nabla_{M_h^k} \varphi_h) : \nabla_{M_h^k} \tilde{W}_h^{k+1} = 0, \end{aligned}$$

$$(81) \quad \int_{M_h^k} \tilde{Y}_h^{k+1} \cdot \psi_h + \nabla_{M_h^k} \tilde{u}_h^{k+1} : \nabla_{M_h^k} \psi_h = 0,$$

$$(82) \quad \int_{M_h^k} \tilde{W}_h^{k+1} \cdot \xi_h - (Y_h^k \cdot N_h^k)^{p-2} \tilde{Y}_h^{k+1} \cdot \xi_h = 0,$$

$$(83) \quad \int_{M_h^k} (dA_h^{k+1} - dA_h^k) = A_0,$$

$$(84) \quad \int_{M_h^k} (\tilde{u}_h^{k+1} - u_h^k) \cdot N_h^k = 3V_0,$$

for all  $\varphi_h, \psi_h, \xi_h \in H^1(S_h)$ .

**Remark 6.1.** As noted in [2], it is useful to employ a trick to make this discretization more numerically stable. In particular, since the identity  $\nabla_M \cdot \varphi = \nabla_M u : \nabla_M \varphi$  holds in the continuous setting, the divergence of  $\varphi$  in the expression above is implemented as

$$(85) \quad \nabla_{M_h^k} \cdot \varphi_h = \nabla_{M_h^k} \tilde{u}_h^{k+1} : \nabla_{M_h^k} \varphi_h,$$

which significantly improves the stability of the temporal discretization.

Similarly, given the output positions  $\tilde{u}_h^{k+1}$  of the above system, the quasi-conformal regularization Problem 4.3 desires to compute  $u_h^{k+1}, \rho_h^{k+1}$  satisfying the system

$$(86) \quad \int_{M_h^{k+1}} \rho_h^{k+1} (\varphi_h \cdot N_h^{k+1}) + (\nabla_{M_{h,2}^{k+1}} u_h^{k+1} - N_h^{k+1} \times \nabla_{M_{h,1}^{k+1}} u_h^{k+1}) \cdot (\nabla_{M_{h,2}^{k+1}} \varphi_h - N_h^{k+1} \times \nabla_{M_{h,1}^{k+1}} \varphi_h) \\ + (\nabla_{M_{h,1}^{k+1}} u_h^{k+1} + N_h^{k+1} \times \nabla_{M_{h,2}^{k+1}} u_h^{k+1}) \cdot (\nabla_{M_{h,1}^{k+1}} \varphi_h + N_h^{k+1} \times \nabla_{M_{h,2}^{k+1}} \varphi_h) = 0,$$

$$(87) \quad \int_{M_h^{k+1}} (u_h^{k+1} - \tilde{u}_h^{k+1}) \cdot N_h^{k+1} = \varepsilon \rho_h^{k+1}.$$

**Remark 6.2.** This system can be overdetermined on triangular meshes, so a penalty parameter  $\varepsilon$  has been introduced in equation (87), on the order of  $\varepsilon = 10^{-4}$ . Since exact conformality is not required by the regularization procedure, this additional flexibility causes no issue in practice.

Once the mesh has been regularized, the new curvature information  $Y_h^{k+1}$  and  $W_h^{k+1}$  are computed through solving the equations

$$(88) \quad \int_{M_h^{k+1}} Y_h^{k+1} \cdot \psi_h + \nabla_{M_h^{k+1}} u_h^{k+1} : \nabla_{M_h^{k+1}} \psi_h = 0,$$

$$(89) \quad \int_{M_h^{k+1}} W_h^{k+1} \cdot \xi_h - (Y_h^k \cdot N_h^k)^{p-2} Y_h^{k+1} \cdot \xi_h = 0.$$

Successive solution of the three systems above constitutes one full step of the algorithm for implementing the closed surface p-Willmore flow with mesh regularization. More concisely, the algorithm is presented as follows.

**Algorithm 6.3.** (*Closed surface p-Willmore flow with quasi-conformal mesh regularization*)

- (1) Given the initial surface positions  $u_h^0$ , generate the curvature data  $Y_h^0, W_h^0$  by solving (88) and (89).
- (2) For integer  $0 \leq k \leq T/\tau$ , evolve the surface according to the following loop
  - (a) Solve the weak form equations in Problem 3.6 (discretized above) to flow the surface until time  $(k+1)\tau$ , computing the necessary positions  $\tilde{u}_h^{k+1}$ , curvatures  $\tilde{Y}_h^{k+1}, \tilde{W}_h^{k+1}$ , and Lagrange multipliers  $\lambda_h^{k+1}$  and  $\mu_h^{k+1}$ .
  - (b) Minimize distortion of the new surface mesh  $\tilde{u}_h^{k+1}$  by solving (86) and (87), yielding positions  $u_h^{k+1}$ .
  - (c) Compute the updated curvature information  $Y_h^{k+1}$  and  $W_h^{k+1}$  from  $u_h^{k+1}$  using again (88) and (89).

This completes one step of the algorithm, which is repeated until a minimizing surface mesh is obtained.

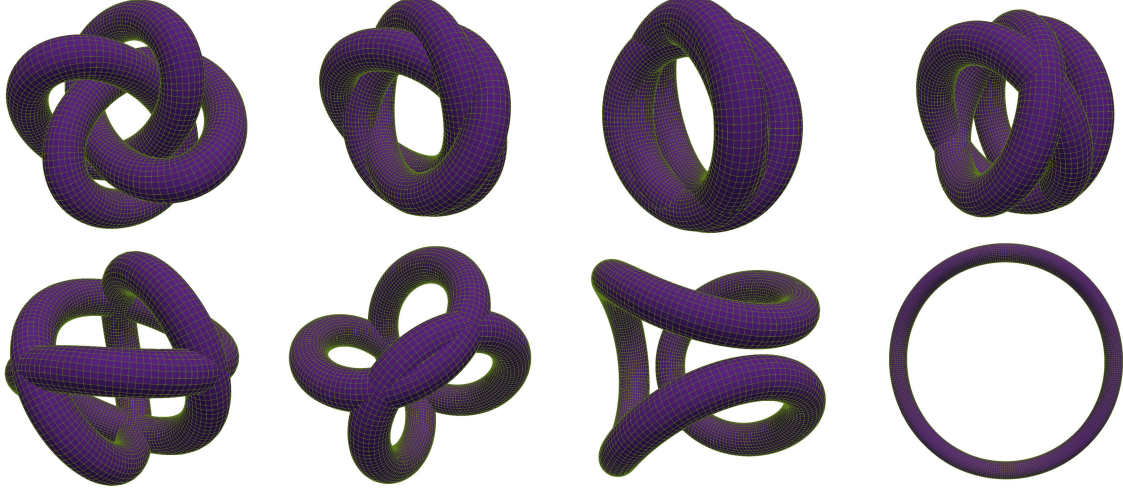


FIGURE 9. Surface area and volume constrained 2-Willmore flow with mesh regularization, applied to a (3,4)-torus knot.

**Conclusion:** The p-Willmore flow with quasi-conformal mesh regularization provides a versatile tool that can be used to study several curvature flows of interdisciplinary interest including MCF, GCF, and the Willmore flow. In particular, the algorithm presented here provides a new and powerful device for visualizing the p-Willmore flow of closed surfaces subject to geometric constraints. Further, a quasi-conformal mesh regularization procedure has been introduced which inhibits mesh degradation along this flow, and allows for many computational surfaces to evolve completely to minima that would be otherwise unreachable (e.g. Figures 7 and 9). Since this procedure can be generally applied to any two-dimensional mesh, it will surely also find utility outside of the realm of evolving surfaces—paving the way for possible future work. Finally, please note that the many examples displayed throughout this paper have been implemented using the freely-available finite element multiphysics solver FEMuS [26].

**Acknowledgments:** The authors would like to acknowledge Dr. Magdalena Toda and Dr. Hung Tran for their many suggestions in developing numerical models for the p-Willmore flow, and Dr. Giorgio Bornia, who assisted with the implementation of .stl and .ply files in the FEMuS library. Moreover, the meshes in Figures 3, 4, and 6 are courtesy of the AIM@SHAPE repository, and the mesh in Figure 9 is courtesy of Microsoft under a CC BY license. Finally, the texture in Figure 1 is courtesy of <https://goldandberry.blogspot.com>, the texture in Figure 2 is due to <https://www.vecteezy.com>, and the textures in Figures 3, 8, 10 are hosted on <https://unsplash.com> courtesy of Mahdis Mousavi, Magdalena Smolnicka, and Orlova Maria respectively.

The research of the second author was partially supported by the NSF grant DMS-1912902.

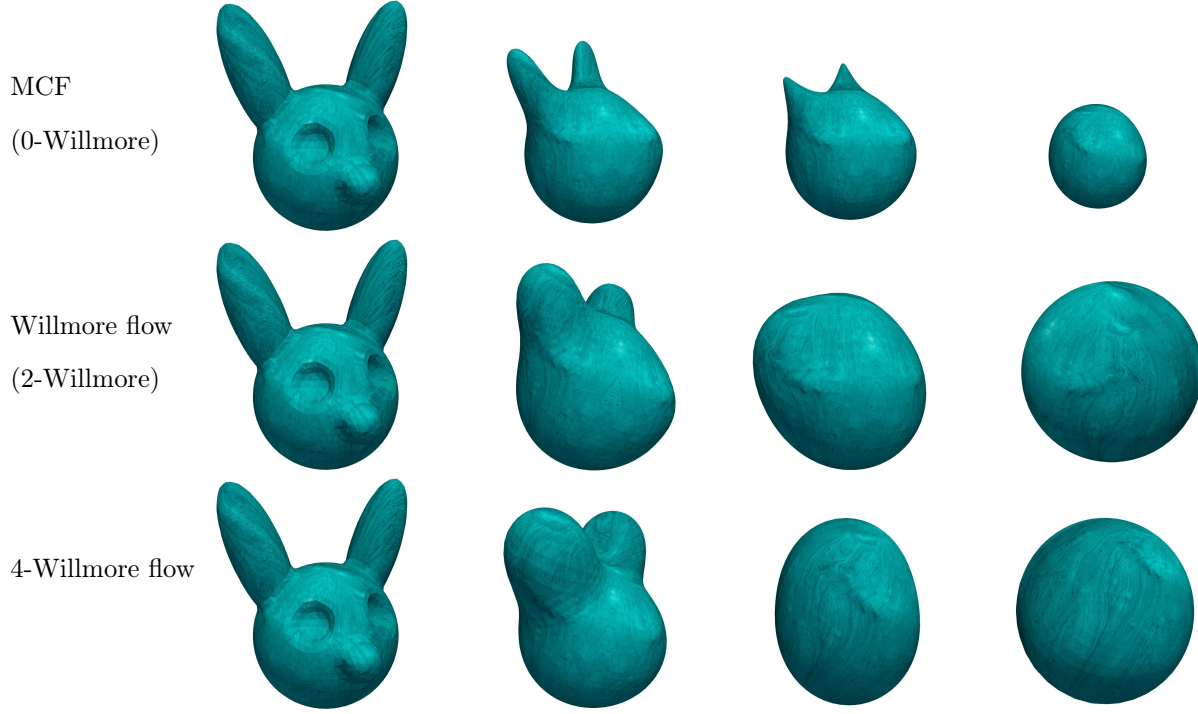


FIGURE 10. p-Willmore flow with mesh regularization applied to a genus 0 bunny mesh when  $p = 0, 2, 4$ .

## REFERENCES

- [1] Anthony Gruber, Magdalena Toda, and Hung Tran. On the variation of curvature functionals in a space form with application to a generalized willmore energy. *Annals of Global Analysis and Geometry*, May 2019.
- [2] G. Dziuk. Computational parametric Willmore flow. *Numerische Mathematik*, 111(1):55, 2008.
- [3] George Kamberov, Franz Pedit, and Ulrich Pinkall. Bonnet pairs and isothermic surfaces. *arXiv preprint dg-ga/9610006*, 1996.
- [4] John W Morgan and Gang Tian. *Ricci flow and the Poincaré conjecture*, volume 3. American Mathematical Soc., 2007.
- [5] MoC Leverett et al. Capillary behavior in porous solids. *Transactions of the AIME*, 142(01):152–169, 1941.
- [6] W. Helfrich. Elastic properties of lipid bilayers: Theory and possible experiments. *Zeitschrift für Naturforschung C*, 28(11-12):693–703, Dec 1973.
- [7] T. J. Willmore. Note on embedded surfaces. *An. Sti. Univ. “Al. I. Cuza” Iasi Sect. I a Mat.(NS) B*, 11:493–496, 1965.
- [8] J. H. White. A global invariant of conformal mappings in space. *Proceedings of the American Mathematical Society*, 38(1):162, 1973.
- [9] J. L. Weiner. On a problem of Chen, Willmore, et al. *Indiana University Mathematics Journal*, 27(1):19–35, 1978.
- [10] A. Mondino. The conformal Willmore functional: A perturbative approach. *Journal of Geometric Analysis*, 23(2):764–811, 2013.
- [11] F. C. Marques and A. Neves. Min-max theory and the Willmore conjecture. *Annals of Mathematics*, 179(2):683–782, 2014.

- [12] B. Athukorallage, G. Bornia, T. Paragoda, and M. Toda. Willmore-type energies and Willmore-type surfaces in space forms. *JP Journal of Geometry and Topology*, 18(2):93, 2015.
- [13] Ernst Kuwert and Reiner Schätzle. The willmore flow with small initial energy. *J. Differential Geom.*, 57(3):409–441, 03 2001.
- [14] H. T. Mondino, A. Nguyen. A gap theorem for Willmore tori and an application to the Willmore flow. *Nonlinear Analysis: Theory, Methods & Applications*, 102:220–225, 2014.
- [15] K. Crane, U. Pinkall, and P. Schröder. Robust fairing via conformal curvature flow. *ACM Trans. Graph.*, 32, 2013.
- [16] G. Dziuk and C.M. Elliott. Finite element methods for surface pdes. *Acta Numerica*, 22:289–396, 2013.
- [17] P. Joshi and C. Séquin. Energy minimizers for curvature-based surface functionals. *Computer-Aided Design and Applications*, 4(5):607–617, 2007.
- [18] Keenan Crane and Max Wardetzky. A glimpse into discrete differential geometry. *Notices of the American Mathematical Society*, 64(10):1153–1159, November 2017.
- [19] Marc Droske and Martin Rumpf. A level set formulation for willmore flow. *Interfaces and free boundaries*, 6(3):361–378, 2004.
- [20] K. Deckelnick and G. Dziuk. Error analysis of a finite element method for the willmore flow of graphs. *Interfaces and free boundaries*, 8(1):21–46, 2006.
- [21] Mark Meyer, Mathieu Desbrun, Peter Schröder, and Alan H Barr. Discrete differential-geometry operators for triangulated 2-manifolds. In *Visualization and mathematics III*, pages 35–57. Springer, 2003.
- [22] Alexander Bobenko. *Discrete differential geometry*. Springer, 2008.
- [23] Xianfeng David Gu, Feng Luo, and S-T Yau. Recent advances in computational conformal geometry. In *IMA International Conference on Mathematics of Surfaces*, pages 189–221. Springer, 2009.
- [24] Klaus Deckelnick, Gerhard Dziuk, and Charles M Elliott. Computation of geometric partial differential equations and mean curvature flow. *Acta numerica*, 14:139–232, 2005.
- [25] Bruno Lévy, Sylvain Petitjean, Nicolas Ray, and Jérôme Maillot. Least squares conformal maps for automatic texture atlas generation. In *ACM transactions on graphics (TOG)*, volume 21, pages 362–371. ACM, 2002.
- [26] Simone Bna Eugenio Aulisa, Giorgio Bornia. Finite element multiphysics solver (femus).
- [27] Carlo Mantegazza. *Lecture notes on mean curvature flow*, volume 290. Springer Science & Business Media, 2011.
- [28] J Lucas Barbosa, Manfredo Do Carmo, and Jost Eschenburg. Stability of hypersurfaces of constant mean curvature in riemannian manifolds. In *Manfredo P. do Carmo-Selected Papers*, pages 291–306. Springer, 2012.
- [29] ZC Ou-Yang and ZC Tu. Overview of the study of complex shapes of fluid membranes, the helfrich model and new applications. *International Journal of Modern Physics B*, 28(01):1330022, 2014.
- [30] Keenan Crane, Ulrich Pinkall, and Peter Schröder. Spin transformations of discrete surfaces. In *ACM Transactions on Graphics (TOG)*, volume 30, page 104. ACM, 2011.
- [31] Mathieu Desbrun, Mark Meyer, and Pierre Alliez. Intrinsic parameterizations of surface meshes. In *Computer graphics forum*, volume 21, pages 209–218. Wiley Online Library, 2002.
- [32] Xianfeng Gu and Shing-Tung Yau. Global conformal surface parameterization. In *Proceedings of the 2003 Eurographics/ACM SIGGRAPH symposium on Geometry processing*, pages 127–137. Eurographics Association, 2003.
- [33] Michael S Floater and Kai Hormann. Surface parameterization: a tutorial and survey. In *Advances in multiresolution for geometric modelling*, pages 157–186. Springer, 2005.

<sup>1,2</sup> DEPARTMENT OF MATHEMATICS AND STATISTICS, TEXAS TECH UNIVERSITY, LUBBOCK, TX 79409, USA.